Contribution from the Departments of Chemistry, University of Minnesota, Minneapolis, Minnesota 55455, Georgetown University, Washington, D.C. 20057, and University of New Orleans, New Orleans, Louisiana 70122

Iron–Oxo Aggregates. Binuclear and Tetranuclear Complexes of *N,N,N′,N′*-Tetrakis(2-benzimidazolylmethyl)-2-hydroxy-1,3-diaminopropane

Qiuhao Chen,[†] John B. Lynch,[†] Pedro Gomez-Romero,[‡] Ahmed Ben-Hussein,[‡] Geoffrey B. Jameson,*[,‡] Charles J. O'Connor,[§] and Lawrence Que, Jr.*[,†]

Received September 11, 1987

Two types of iron(III) complexes of *N,N,N′,N′*-tetrakis(2-benzimidazolylmethyl)-2-hydroxy-1,3-diaminopropane (L) and its 1-ethylbenzimidazole (L-Et) and 5,6-dimethyl (L-Me_2) derivatives have been isolated from organic solvents and characterized by NMR, IR, and magnetic susceptibility data. Two tetranuclear compounds have been structurally characterized in the space group $P\bar{1}$, $[Fe_4O_2L_2(O_2CC_6H_5)_2](ClO_4)_2(OTs)_2{\cdot}6CH_3CN{\cdot}2CH_3OH$ (a = 14.719 (11) Å, b = 14.784 (11) Å, c = 16.716 (25) Å, α = 66.53 (9)°, β = 65.03 (9)°, γ = 85.70 (6)°) and $[Fe_4O_2(L\text{-}Et)_2(O_2CCH_3)_2](BF_4)_4{\cdot}x$(solvate) ($a$ = 14.825 (5) Å, b = 15.481 (5) Å, c = 12.794 (3) Å, α = 94.21 (2)°, β = 106.25 (2)°, γ = 92.10 (3)°). Both complexes consist of two $[Fe_2L(O_2CR)]$ units connected by nearly linear oxo bridges to form a nearly square array of iron atoms. The iron atoms in the $[Fe_2L(O_2CR)]$ unit are bridged by the alkoxo group from the septadentate ligand and the carboxylate. These complexes and similar derivatives exhibit strong antiferromagnetic coupling presumably via the oxo bridges as reflected by the weak magnetic susceptibility and the relatively small NMR isotropic shifts. The other type of complex obtained has the general formulation $[Fe_2L(O_2CR)_2]X_3$. The iron(III) centers are coupled antiferromagnetically via the alkoxo bridge with $J = -25$ cm^{-1}. On the basis of IR and NMR observations, the iron coordination in this complex is postulated to consist of the N_3O donor groups from L and the oxygen atoms from bridging carboxylates, which are coordinated quite unsymmetrically. This unsymmetric bridging is attributed to the stereochemical constraints imposed by the short length of the hydroxypropane unit that links the two N_3 units of L in the (μ-alkoxo)bis(μ-benzoato)diiron(III) unit. The factors that govern formation of the binuclear complex or the tetranuclear complex are not understood.

There is considerable current interest in understanding the coordination chemistry of metal sites in iron–oxo proteins,[1] such as hemerythrin,[2] ribonucleotide reductase,[3] purple acid phosphatases,[4] and ferritin.[5] The first three proteins contain binuclear iron sites in which an oxo group serves to bridge iron(III) centers in one of the forms of the protein, while ferritin consists of a large polynuclear iron oxide core surrounded by a protein shell. Hemerythrin (Hr), the prototype of the binuclear iron–oxo protein, has been shown crystallographically to have a (μ-oxo)bis(μ-carboxylato)diiron(III) core in its met and oxy forms.[6] Five of the remaining six coordination positions are taken up by histidines, while the sixth site is occupied by azide and hydroperoxide in metHrN_3 and oxyHr, respectively. Ribonucleotide reductase from *Escherichia coli* and the beef spleen purple acid phosphatase have both been proposed to have a similar triply bridged diiron(III) unit on the basis of EXAFS studies.[7,8]

Models for the binuclear iron–oxo site have been reported with use of a variety of face-capping tridentate ligands,[9–12] indicating that such triply bridged diiron structures are thermodynamically stable. Efforts to increase the iron–oxo core size have resulted in the identification of a number of oligomeric iron–oxo complexes with core compositions of Fe_3O,[13] Fe_4O_2,[1,14] $Fe_4O_2(OH)_2$,[15] $Fe_6O_2(OH)_2$,[16a] $Fe_8O_2(OH)_{12}$,[16b] and $Fe_{11}O_6(OH)_6$.[17] The trinuclear and tetranuclear complexes, in particular, involve polydentate ligands that span over at least two metal centers.

Our interest in iron–oxo proteins has led us to explore the iron(III) chemistry of *N,N,N′,N′*-tetrakis(2-benzimidazolylmethyl)-2-hydroxy-1,3-diaminopropane (L) and its 1-ethylbenzimidazole (L-Et) and 5,6-dimethylbenzimidazole (L-Me_2) derivatives. This ligand has been useful for the synthesis of models for methemocyanin, where the copper centers are bridged by the alkoxide oxygen and anions such as azide, acetate, and nitrite.[18a] Manganese complexes have also been synthesized and proposed as models for the manganese pseudocatalase site.[18b] The ferric nitrate complex of L, $[Fe_2L(NO_3)_5]$, has been previously reported.[18c] In our studies, we have synthesized binuclear and tetranuclear iron complexes of L in the presence of carboxylates, with stoichiometries of $[Fe_2L(O_2CR)_2]X_3$ and $[Fe_4O_2L_2(O_2CR)_2]X_4$; crystal structures of two tetranuclear complexes are discussed, and the physical properties of the two types of complexes are compared.

Experimental Section

Ligands. 2-Hydroxy-1,3-diaminopropanetetraacetic acid, 2-aminoaniline, 4,5-dimethyl-2-aminoaniline, and all the carboxylic acids were obtained from Aldrich. The aminoanilines were sublimed before use,

[†] University of Minnesota.
[‡] Georgetown University.
[§] University of New Orleans.

(1) Lippard, S. J. *Chem. Br.* **1986**, 222–229.
(2) Klotz, I. M.; Kurtz, D. M., Jr. *Acc. Chem. Res.* **1984**, *17*, 16–22. Sanders-Loehr, J.; Loehr, T. M. *Adv. Inorg. Biochem.* **1979**, *1*, 235–252.
(3) Reichard, P.; Ehrenberg, A. *Science (Washington, D.C.)* **1983**, *221*, 514–519.
(4) Antanaitis, B. C.; Aisen, P. *Adv. Inorg. Biochem.* **1983**, *5*, 111–136.
(5) Theil, E. C. *Adv. Inorg. Biochem.* **1983**, *5*, 1–38.
(6) Stenkamp, R. E.; Sieker, L. C.; Jensen, L. H. *J. Am. Chem. Soc.* **1984**, *106*, 618–622. Hendrickson, W. A. In *Invertebrate Oxygen-Binding Proteins: Structure, Active Site, and Function*; Lamy, J., Lamy, J., Eds.; Marcel Dekker: New York, 1981; pp 503–515.
(7) Scarrow, R. C.; Maroney, M. J.; Palmer, S. M.; Que, L., Jr.; Salowe, S. P.; Stubbe, J. *J. Am. Chem. Soc.* **1986**, *108*, 6832–6834.
(8) Kauzlarich, S. M.; Teo, B. K.; Zirino, T.; Burman, S.; Davis, J. C.; Averill, B. A. *Inorg. Chem.* **1986**, *25*, 2781–2785.
(9) Armstrong, W. H.; Spool, A.; Papefthymiou, G. C.; Frankel, R. B.; Lippard, S. J. *J. Am. Chem. Soc.* **1984**, *106*, 3653–3667.
(10) Wieghardt, K.; Pohl, K.; Gebert, K. *Angew. Chem., Int. Ed. Engl.* **1983**, *22*, 727–728.
(11) Toftlund, H.; Murray, K. S.; Zwack, P. R.; Taylor, L. F.; Anderson, O. P. *J. Chem. Soc., Chem. Commun.* **1986**, 191–192.
(12) (a) Gomez-Romero, P.; Casan-Pastor, N.; Ben-Hussein, A.; Jameson, G. B. *J. Am. Chem. Soc.*, in press. (b) Gomez-Romero, P. Ph.D. Thesis, Georgetown University, 1987.
(13) (a) Gorun, S.; Lippard, S. J. *J. Am. Chem. Soc.* **1985**, *107*, 4568–4570. Gorun, S. M.; Papaefthymiou, G. C.; Frankel, R. B.; Lippard, S. J. *J. Am. Chem. Soc.* **1987**, *109*, 4244–4255. (b) Thundathil, R. V.; Holt, E. M.; Holt, S. L.; Watson, K. J. *J. Am. Chem. Soc.* **1977**, *99*, 1818–1823.
(14) (a) Jameson, D. L.; Xie, M.; Hendrickson, D. N.; Potenza, J. A.; Schugar, H. J. *J. Am. Chem. Soc.* **1987**, *109*, 740–746. (b) Ponomarev, V. I.; Atovmyan, L. O.; Bobkova, S. A.; Turtê, K. J. *Dokl. Akad. Nauk SSSR* **1984**, *274*, 368–372. (c) Armstrong, W. H.; Roth, M. E.; Lippard, S. J. *J. Am. Chem. Soc.* **1987**, *109*, 6318–6326.
(15) Murch, B. P.; Boyle, P. D.; Que, L., Jr. *J. Am. Chem. Soc.* **1985**, *107*, 6728–6729. Murch, B. P.; Bradley, F. C.; Boyle, P. D.; Papaefthymiou, V.; Que, L., Jr. *J. Am. Chem. Soc.*, in press.
(16) (a) Gerbeleu, N. V.; Batsanov, A. S.; Timko, G. A.; Struchnov, Y. T.; Indrichan, K. M.; Popovich, G. A. *Dokl. Akad. Nauk SSSR* **1987**, *293*, 364. (b) Wieghardt, K.; Pohl, K.; Jibril, I.; Huttner, G. *Angew. Chem., Int. Ed. Engl.* **1984**, *23*, 77–78.
(17) Gorun, S.; Lippard, S. J. *Nature (London)* **1986**, *319*, 666–668. Gorun, S. M.; Papaefthymiou, G. C.; Frankel, R. B.; Lippard, S. J. *J. Am. Chem. Soc.* **1987**, *109*, 3337–3348.
(18) (a) McKee, V.; Zvagulis, M.; Dagdigian, J. V.; Patch, M. G.; Reed, C. A. *J. Am. Chem. Soc.* **1984**, *106*, 4765–4772. McKee, V.; Zvagulis, M.; Reed, C. A. *Inorg. Chem.* **1985**, *24*, 2914–2919. (b) Mathur, P.; Crowder, M.; Dismukes, G. C. *J. Am. Chem. Soc.* **1987**, *109*, 5227–5233. (c) Nishida, Y.; Takeuchi, M.; Shimo, H.; Kida, S. *Inorg. Chim. Acta* **1984**, *96*, 115–119.

0020-1669/88/1327-2673$01.50/0 © 1988 American Chemical Society

while all other reagents were used without further purification. The binucleating ligands L and L-Et were synthesized by following published procedures.[17] For L-Me_2, 4,5-dimethyl-2-aminoaniline was used in place of 2-aminoaniline and the product yielded a satisfactory NMR spectrum. ^1H NMR of L(CD_3CN/DMSO-d_6): δ 7.3 (AA'BB', 16 H), 4.84 (broad, 5 H), 3.94 (m, 9 H), 2.02 (m, 4 H). ^1H NMR of L-Me_2 (CD_3CN/DMSO-d_6): δ 7.19 (s, 8 H), 4.84 (broad, 5 H), 3.94 (m, 9 H), 2.27 (s, 24 H), 2.02 (m, 4 H).

$[Fe_2L(OBz)_2](ClO_4)_3$.[19] A 0.3054-g (0.5-mmol) amount of L, 0.1221 g (1 mmol) of benzoic acid, and 0.139 mL (1 mmol) of Et_3N were dissolved in 10 mL of MeOH, and the mixture was then cooled in an ice bath. A 0.3736-g (1-mmol) amount of $Fe(ClO_4)_3 \cdot H_2O$ was added to the cold solution. The mixture was stirred, the crystals dissolved completely, giving rise to a wine-colored solution. The solution was allowed to stand at room temperature for 1–2 days, and orange needles of the complex were obtained. The use of L-Et in place of L or substituted benzoic acids in place of benzoic acid also resulted in the syntheses of other binuclear complexes of similar stoichiometry. No binuclear complex could be obtained for L-Me_2 under these conditions. $[Fe_2L(OBz)_2](ClO_4)_3$: yield 73%. Anal. Calcd for $C_{49}H_{43}Cl_3Fe_2N_{10}O_{17}$: C, 46.63; H, 3.44; Cl, 8.43; Fe, 8.85; N, 11.09. Found: C, 46.50; H, 3.62; Cl, 8.19, Fe, 8.64; N, 11.13. $[Fe_2L(4\text{-}F\text{-}C_6H_4CO_2)_2](ClO_4)_3$: yield 73%. Anal. Calcd for $C_{49}H_{41}Cl_3F_2Fe_2N_{10}O_{17}$: C, 45.34; H, 3.19; Cl, 8.19; Fe, 8.61; N, 10.97. Found: C, 45.64; H, 3.46; Cl, 7.94; Fe, 8.66; N, 10.90. $[Fe_2L\text{-}Et\text{-}(OBz)_2](ClO_4)_3$: yield 72%. Anal. Calcd for $C_{57}H_{59}Cl_3Fe_2N_{10}O_{17}$: C, 49.82; H, 4.85; Fe, 8.13; N, 10.19. Found: C, 50.00; H, 4.43; Fe, 8.37; N, 10.34. Other complexes that were made by this method but not analyzed include $[Fe_2L(O_2CR)_2](ClO_4)_3$, where R = $-C_6H_4$-4-OCH_3, $-C_6H_4$-4-Br, $-C_6H_4$-4-CF_3, and $-C_6H_3$-3,5-Cl_2. Attempts to synthesize the binuclear complexes where R = $-C_2H_5$ and $-C_6H_4$-4-CH_3 by using the above procedure resulted in the formation of the corresponding tetranuclear species, as determined by their NMR spectra.

$[Fe_4O_2L_2(OBz)_2]X_4$. Tetranuclear complexes of L were obtained by mixing 0.48 g (0.38 mmol) $[Fe_2L(OBz)_2](ClO_4)_3$ of in 60 mL of CH_3CN with 0.237 g of NaOTs (1.25 mmol) in 15 mL of MeOH; when the mixture stood 1 week, crystals of the ditosylate diperchlorate salt formed. These were washed with cold MeOH, vacuum-dried, and used for the noncrystallographic experiments. $[Fe_4O_2L_2(OBz)_2](ClO_4)_2(OTs)_2 \cdot CH_3OH \cdot 3H_2O$: yield 29%. Anal. Calcd for $C_{99}H_{100}Cl_2Fe_4N_{20}O_{26}S_2$: C, 50.72; H, 4.30; Fe, 9.53; N, 11.95. Found: C, 50.70; H, 4.23; Fe, 9.68, N, 11.70. $[Fe_4O_2(L\text{-}Me_2)_2(O_2CC_6H_4\text{-}4\text{-}F)_2](ClO_4)_2(OTs)_2$ was also obtained in the same manner.

Tetranuclear complexes of L-Me_2 were obtained by dissolving 0.542 g (0.75 mmol) of L-Me_2, 0.183 g (1.5 mmole) of benzoic acid, and 0.315 mL (2.25 mmol) of Et_3N in 84 mL of absolute EtOH. The solution was cooled in an ice bath, and 0.560 g (ca. 1.5 mmol) of $Fe(ClO_4)_3 \cdot xH_2O$ was added. The solution was allowed to stand at room temperature for 2 days, and brown needles were deposited in the flask. These were collected, washed with absolute EtOH, and dried under vacuum. $[Fe_4O_2(L\text{-}Me_2)_2(OBz)_2](ClO_4)_4 \cdot 4H_2O$: yield 60%. Anal. Calcd for $C_{100}H_{116}Cl_4Fe_4N_{20}O_{28}$: C, 49.81; H, 4.86; Cl, 5.88; Fe, 9.26; N, 11.61. Found: C, 49.81; H, 4.81; Cl, 5.81; Fe, 9.32; N, 11.59. Other tetranuclear complexes that were obtained by direct synthesis but not analyzed include $[Fe_4O_2(L\text{-}Me_2)_2(O_2CC_6H_4\text{-}4\text{-}F)_2](ClO_4)_4$, $[Fe_4O_2(L\text{-}Me_2)_2(O_2CC_6H_3\text{-}3,5\text{-}Cl_2)_2](ClO_4)_4$, $[Fe_4O_2(L\text{-}Me_2)_2(OAc)_2](ClO_4)_4$, $[Fe_4O_2L_2(O_2CC_6H_4\text{-}4\text{-}CH_3)_2](ClO_4)_4$, and $[Fe_4O_2L_2(OPr)_2](BPh_4)_4$. The last two complexes were formed by using a 1:2:2:2 ratio of ligand, ferric ion, carboxylate, and base, as in the synthesis for the binuclear complexes; the propionate complex was isolated by metathesis with $NaBPh_4$.

The tetranuclear complex was also obtaind by an alternative procedure as follows: To a solution of L-Et (1 mmol) and triethylamine (1 mmol) in ethanol (30 mL) was added $Fe(OAc)_2$ (2 mmol) and $NaBF_4$ (2 mmol) consecutively under N_2. The resulting brown-green solution was exposed to air to cause a color change to dark brown. After several days the brown precipitate was collected, air-dried, and then recrystallized from CH_3CN to yield $[Fe_4O_2(L\text{-}Et)_2(OAc)_2](BF_4)_4 \cdot 8H_2O$. Anal. Calcd for $C_{90}H_{120}B_4F_{16}Fe_4N_{20}O_{16}$: C, 46.83; H, 5.24; Fe, 9.68; N, 12.14. Found: C, 46.78; H, 5.07; Fe, 9.79; N, 12.41. UV–vis-near-IR (nm): 360 (sh, ϵ 5362 M^{-1} cm^{-1}/Fe), 945 (ϵ 2 M^{-1} cm^{-1}/Fe).

(19) Abbreviations used: OBz, benzoate; OTs, tosylate; OAc, acetate; OPr, propionate; SALPAH, *N*-(3-hydroxypropyl)salicylideneamine; $(sal)_3$trien, trisalicylidenetriethylenetetramine; HPTA, *N,N'*-bis[*N,N*-bis(carboxymethyl)glycyl]-2-hydroxy-1,3-diaminopropane; $HB(pz)_3$, hydrotripyrazolylborate; NTA, *N,N*-bis(carboxymethyl)glycine; DBC, 3,5-di-*tert*-butylcatecholate dianion; HEDTA, *N*-(2-hydroxyethyl)-*N'*-(carboxymethyl)-*N,N'*-ethylenebis(glycine); 5-Me-HXTA, *N,N'*-(2-hydroxy-1,3-xylylene)bis[*N*-(carboxymethyl)glycine]; EDTA, *N,N'*-ethylenebis[*N*-(carboxymethyl)glycine]; N5, *N,N,N'*-tris(2-benzimidazolyl)methyl-*N'*-(2-hydroxyethyl)-1,2-diaminoethane; TIEO, 1,1,2-tris(1-methylimidazol-2-yl)-1-hydroxyethane; salhis, 4-[2-(salicylideneamino)ethyl]imidazole; $TTPPPH_2$, 5,10,15,20-tetrakis(2,4,6-triphenylphenyl)porphyrin; N3, bis(2-benzimidazolylmethyl)amine; LXy, *N,N'*-(2-hydroxy-1,3-xylylene)bis[bis(2-benzimidazolylmethyl)-amine].

Table I. Crystallographic and Refinement Data for $[Fe_4O_2L_2(OBz)_2](ClO_4)_2(OTs)_2 \cdot 6CH_3CN \cdot 2CH_3OH$ (**1**) and $[Fe_4O_2(L\text{-}Et)_2(OAc)_2](BF_4)_4$ (**2**)

formula	$C_{98}H_{106}Cl_2Fe_4N_{26}O_{24}S_2$	$C_{90}H_{104}B_4F_{16}Fe_4N_{20}O_8$
M_r	2390.52	2264.68
space group	$P\bar{1}$	$P\bar{1}$
a, Å	14.719 (11)	14.825 (4)
b, Å	14.784 (11)	15.481 (5)
c, Å	16.716 (25)	12.794 (3)
α, deg	66.53 (9)	94.21 (2)
β, deg	65.03 (9)	106.25 (2)
γ, deg	85.70 (6)	92.10 (3)
V, Å^3	3005 (5)	2807 (3)
temp, °C	−74	23
Z	1	1
D_{calcd}, g/cm^3	1.321 (2)	1.34
radiation used	Mo Kα (λ = 0.71073 Å)	Mo Kα
max (sin θ)/λ	0.66	0.53
cryst size, mm^3	0.4 × 0.4 × 0.6	0.15 × 0.20 × 0.60
μ, cm^{-1}	6.23	5.92
transmission factors	0.894–0.999[c]	0.88–0.92[d]
no. of rflns measd	14603	5204
no. of rflns used[a]	10010 [$(F_o)^2 \geq 3\sigma(F_o)^2$]	2171
no. of variables used	523	325
R[b]	0.077	0.090
R_w[b]	0.104	0.100
GOF[b]	2.931	2.30
p[a]	0.05	0.05

[a] The intensity data for **1** were processed as described in: *CAD 4 and SDP-PLUS User's Manual*; B. A. Frenz: College Station, TX, 1982. The net intensity $I = [K(NPI)](C - 2B)$, where $K = 20.1166$ (attenuator factor), NPI = ratio of fastest possible scan rate to scan rate for the measurement, C = total count, and B = total background count. For **2**, intensity data were collected on a Picker FACS-I diffractometer using the NRC-Canada software (E. Crabe), which includes on-line profile analysis. The standard deviation in the net intensity is given by $[\sigma(I)]^2 = (K/NPI)^2[C + 4B + (PI)^2]$, where P is a factor used to downweight intense reflections. The observed structure factor amplitude F_o is given by $F_o = (I/Lp)^{1/2}$, where Lp = Lorentz and polarization factors. The $\sigma(I)$'s were converted to the estimated errors in the relative structure factors $\sigma(F_o)$ by $\sigma(F_o) = {}^1/_2[\sigma(I)/I]F_o$. [b] The function minimized was $\sum w(|F_o| - |F_c|)^2$, where $w = 1/[\sigma(F_o)]^2$. The unweighted and weighted residuals are defined as $R = (||F_o| - |F_c||)/\sum|F_o|$ and $R_w = [(\sum w(|F_o| - |F_c|))^2/(\sum|F_o|)^2]^{1/2}$. The error is an observation of unit weight (GOF) is $[\sum w(|F_o| - |F_c|)^2/(NO - NV)]^{1/2}$, where NO and NV are the numbers of observations and variables, respectively. [c] ψ scans were run and absorption corrections were applied by using EAC (part of the SDP-PLUS software package). [d] By Gaussian integration: no correction applied.

Crystallographic Studies. Single crystals of $[Fe_4O_2L(OBz)_2](ClO_4)_2(OTs)_2$ (**1**) were obtained by dissolving $[Fe_2L(OBz)_2](ClO_4)_3$ in CH_3CN/MeOH (4:1) in the presence of NaOTs and allowing the solution to stand for 1 week. Data were collected at the Crystallography Facility of the University of Minnesota Chemistry Department on an Enraf-Nonius CAD4 diffractometer at −74 °C on a crystal coated with a viscous high-molecular-weight hydrocarbon to prevent solvent loss. Crystallographic and refinement data are summarized in Table I. A large crystal (0.4 × 0.4 × 0.6 mm) was used in order to get data to θ = 28°. It is our experience with large crystals at low temperature that errors in the cell constants are about twice as large as what we would expect in a smaller crystal. It is not clear why this happens, but it does, and we have sacrificed accuracy in cell constants for more data. It was suggested by a reviewer that our cell was misassigned. At the time that the data were collected, it was recognized that the transformation matrix $110/1\bar{1}0/00\delta in1$ leads to a *C*-centered cell with a = 21.630 Å, b = 20.065 Å, c = 16.716 Å, α = 90.93°, β = 124.02°, and γ = 90.25°. However, the pattern of intensities showed that this possibly monoclinic cell was only accidental and that the true symmetry was triclinic.

The iron atoms were first located by using Patterson maps; the other atoms were then found by difference Fourier methods and refined anisotropically. The accuracy of this structure (R = 7.7%, R = 10.4%) was limited by the inefficient packing of the bulky cation and the smaller

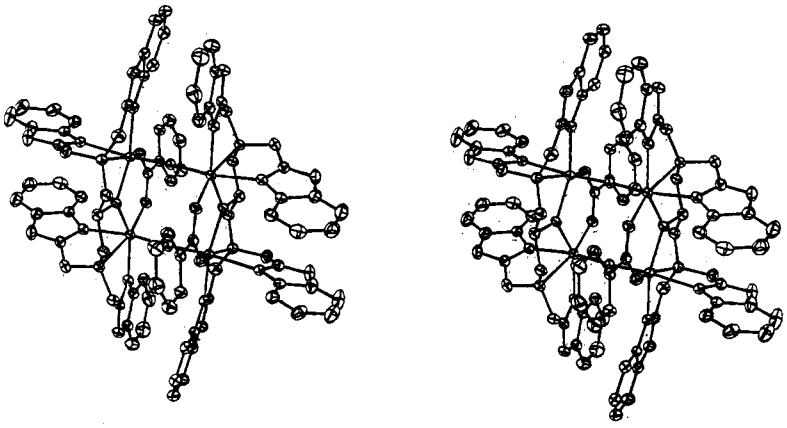

Figure 1. Stereoview of the complex $[Fe_4O_2L_2(OBz)_2]^{4+}$.

Table II. Atomic Coordinates for the Non-Hydrogen Atoms of $[Fe_4O_2L_2(OBz)_2](ClO_4)_2(OTs)_2$ (**1**)

atom	x	y	z	B, Å²	atom	x	y	z	B, Å²
Fe1	0.06246 (4)	0.18365 (4)	−0.05335 (4)	1.52 (1)	C8C	0.5629 (4)	0.1906 (4)	−0.1709 (4)	3.3 (1)
Fe2	−0.17334 (4)	0.02960 (4)	0.07960 (4)	1.52 (1)	C9C	0.5539 (4)	0.2045 (4)	−0.2540 (4)	3.1 (1)
O12	−0.0549 (2)	0.1056 (2)	0.0202 (2)	1.92 (6)	C11D	0.1961 (4)	−0.1103 (3)	−0.2272 (3)	2.17 (9)
O	0.1264 (2)	0.1042 (2)	−0.1312 (2)	1.64 (6)	N1D	0.2492 (3)	−0.1574 (3)	−0.0964 (2)	1.89 (8)
C0	0.1292 (3)	0.1385 (3)	−0.2250 (3)	1.74 (9)	C2D	0.2482 (3)	−0.1731 (3)	−0.1687 (3)	1.92 (9)
C1	0.0401 (3)	0.1961 (3)	−0.2263 (3)	2.11 (9)	N3D	0.2955 (3)	−0.2521 (3)	−0.1795 (3)	2.22 (8)
N1	0.0437 (3)	0.2741 (2)	−0.1930 (2)	1.84 (8)	C4D	0.3274 (3)	−0.2927 (3)	−0.1064 (3)	2.2 (1)
C11A	0.1296 (3)	0.3519 (3)	−0.2658 (3)	2.2 (1)	C5D	0.2988 (3)	−0.2323 (3)	−0.0547 (3)	2.05 (9)
N1A	0.1975 (3)	0.2944 (2)	−0.1426 (2)	1.77 (7)	C6D	0.3169 (3)	−0.2544 (3)	0.0263 (3)	2.3 (1)
C2A	0.2078 (3)	0.3488 (3)	−0.2313 (3)	2.05 (9)	C7D	0.3619 (4)	−0.3402 (4)	0.0551 (4)	3.0 (1)
N3A	0.2945 (3)	0.4114 (3)	−0.2864 (3)	2.8 (1)	C8D	0.3905 (4)	−0.3999 (4)	0.0033 (4)	3.6 (1)
C4A	0.3429 (3)	0.3989 (4)	−0.2267 (3)	2.6 (1)	C9D	0.3750 (4)	−0.3772 (4)	−0.0783 (4)	3.1 (1)
C5A	0.2809 (3)	0.3248 (3)	−0.1362 (3)	2.01 (9)	O1E	0.1219 (2)	0.1253 (2)	0.0438 (2)	2.11 (7)
C6A	0.3057 (4)	0.3004 (3)	−0.0592 (3)	2.4 (1)	C7E	0.1528 (3)	0.0426 (3)	0.0756 (3)	1.69 (8)
C7A	0.3917 (3)	0.3505 (3)	−0.0743 (4)	2.7 (1)	O2E	0.1725 (2)	−0.0194 (2)	0.0373 (2)	2.00 (7)
C8A	0.4531 (4)	0.4242 (4)	−0.1656 (4)	3.3 (1)	C1E	0.1687 (3)	0.0162 (3)	0.1649 (3)	1.92 (9)
C9A	0.4295 (4)	0.4487 (4)	−0.2425 (4)	3.8 (2)	C2E	0.1936 (4)	−0.0773 (3)	0.2083 (3)	2.3 (1)
C11B	−0.0518 (3)	0.3179 (3)	−0.1642 (3)	2.2 (1)	C3E	0.2101 (4)	−0.1017 (4)	0.2894 (3)	2.9 (1)
N1B	−0.0130 (3)	0.3069 (2)	−0.0312 (2)	1.91 (8)	C4E	0.2030 (4)	−0.0324 (4)	0.3282 (3)	2.8 (1)
C2B	−0.0576 (3)	0.3514 (3)	−0.0890 (3)	2.1 (1)	C5E	0.1776 (4)	0.0606 (4)	0.2853 (3)	2.8 (1)
N3B	−0.1139 (3)	0.4209 (3)	−0.0651 (3)	2.23 (8)	C6E	0.1598 (4)	0.0855 (3)	0.2050 (3)	2.3 (1)
C4B	−0.1065 (3)	0.4207 (3)	0.0148 (3)	2.3 (1)	S1F	0.3604 (3)	−0.2344 (2)	−0.4432 (1)	9.7 (1)
C5B	−0.0431 (3)	0.3492 (3)	0.0362 (3)	2.03 (9)	O1F	0.344 (1)	−0.2876 (5)	−0.4921 (4)	17.3 (4)
C6B	−0.0199 (4)	0.3297 (3)	0.1136 (3)	2.5 (1)	O2F	0.3328 (6)	−0.2957 (3)	−0.3410 (3)	7.0 (2)
C7B	−0.0657 (4)	0.3821 (3)	0.1711 (3)	2.8 (1)	O3F	0.4625 (6)	−0.1859 (6)	−0.4941 (4)	12.7 (2)
C8B	−0.1306 (4)	0.4521 (3)	0.1498 (3)	3.1 (1)	C1F	0.2806 (7)	−0.1407 (5)	−0.4505 (4)	5.3 (2)
C9B	−0.1521 (4)	0.4739 (3)	0.0712 (4)	2.9 (1)	C2F	0.3175 (6)	−0.0415 (5)	−0.4965 (4)	4.4 (2)
C2	0.1273 (3)	0.0508 (3)	−0.2498 (3)	2.05 (9)	C3F	0.2540 (5)	0.0285 (5)	−0.4993 (4)	4.0 (1)
N2	0.2068 (3)	−0.0093 (3)	−0.2317 (2)	1.81 (8)	C4F	0.1504 (5)	0.0028 (6)	−0.4574 (4)	5.3 (2)
C11C	0.3089 (3)	0.0427 (3)	−0.3025 (3)	2.2 (1)	C5F	0.1148 (6)	−0.0945 (7)	−0.4131 (4)	7.0 (2)
N1C	0.3268 (3)	0.0465 (3)	−0.1626 (2)	1.87 (8)	C6F	0.1733 (7)	−0.1651 (6)	−0.4074 (4)	7.7 (2)
C2C	0.3569 (3)	0.0794 (3)	−0.2572 (3)	2.04 (9)	C7F	0.0811 (6)	0.0852 (8)	−0.4652 (5)	7.3 (3)
N3C	0.4417 (3)	0.1439 (3)	−0.3080 (3)	2.51 (9)	Cl1G	−0.1915 (2)	−0.3541 (1)	−0.2268 (1)	5.61 (5)
C4C	0.4711 (3)	0.1511 (3)	−0.2420 (3)	2.4 (1)	O1G	−0.0991 (7)	−0.2805 (5)	−0.2872 (6)	10.8 (3)
C5C	0.3986 (3)	0.0894 (3)	−0.1508 (3)	2.10 (9)	O2G	−0.2178 (7)	−0.3547 (6)	−0.1376 (4)	10.8 (3)
C6C	0.4099 (4)	0.0753 (3)	−0.0676 (3)	2.4 (1)	O3G	−0.1618 (4)	−0.4480 (3)	−0.2265 (4)	6.2 (1)
C7C	0.4943 (4)	0.1275 (4)	−0.0802 (3)	2.9 (1)	O4G	−0.2505 (6)	−0.3230 (6)	−0.2666 (6)	21.1 (2)

anions, resulting in disorder among the anions and solvent molecules as indicated by the large thermal parameters for O1F and O4G. It was not economically feasible to pursue a model that would account for the disorder, particular since the structure of chemical interest, i.e. the cation, did not seem to be significantly affected by the disorder.

Single crystals of $[Fe_4O_2(L\text{-}Et)_2(OAc)_2](BF_4)_4$ (**2**) were obtained by slow recrystallization from CH_3CN. Crystals were quickly isolated and sealed in thin-walled glass capillaries to minimize loss of solvent molecules. Crystallographic and refinement data are summarized in Table I. Intensity data were scaled for a 23% monotonic decrease observed in three regularly monitored standard reflections; there was no evidence for extinction. The structure was solved by direct methods (MULTAN 82 as incorporated in SDP from B. A. Frenz & Associates). The inability to adequately model the reflection intensity for the highly disordered BF_4 anions and solvate molecules led, at low $\lambda^{-1}\sin\theta$ values, to poor agreement among the $|F_c|$ and $|F_o|$ values. Thus, in the final refinements, their contributions to F_c were fixed, as well as those of hydrogen atoms in the ligand L-Et (placed at idealized positions), while the more sharply defined cation was refined by using only those data for which $F_o^2 > 3\sigma(F_o^2)$ and $\lambda^{-1}\sin\theta > 0.25$ Å^{-1}. At higher angles, the relative contribution to F_c from the chemically uninteresting species with high atomic displacement parameters becomes progressively smaller and the inaccuracies in atom parameters for the chemically interesting and well-defined cation induced by an inadequate model for the ill-defined portions are reduced. Thus, we observe that chemically equivalent bond distances and angles in the cation have statistically insignificant differences and the geometry of the benzimidazole moiety conforms closely to that seen in other structures. The values for R and R_w for all data with $F_o^2 > 3\sigma(F_o^2)$ are 0.097 and 0.116.

A stereoview of the cation **1** is shown in Figure 1, while the tetranuclear core is shown in Figure 2, together with the numbering scheme for the core. Cation **2** is very similar (Figure S1, supplementary material). The numbering scheme for the binucleating ligand is shown in Figure S2 (supplementary material). Fractional atomic coordinates for the nonhydrogen atoms of the tetracation and anions for **1** and **2** are listed in Tables II and III, respectively, while selected bond distances and bond angles for both cations are compared in Table IV. Atomic coordinates for the hydrogen atoms and solvent molecules and atomic displacement parameters for **1** are given in Tables S1 and S2, respectively; similarly, atomic coordinates for the hydrogen atoms, anions, and solvent molecules

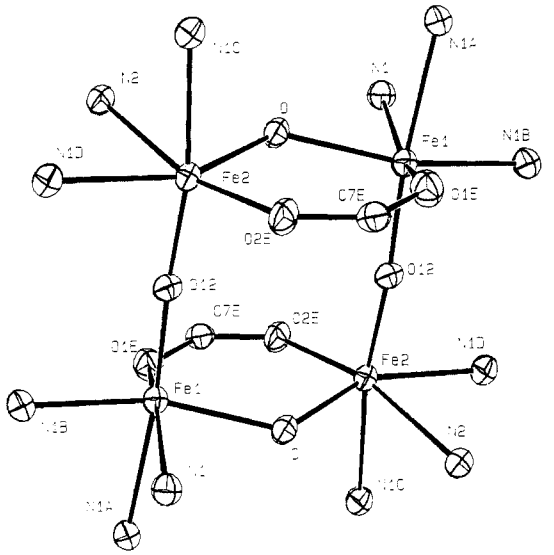

Figure 2. Atom arrangement for the core of $[Fe_4O_2L_2(OBz)_2]^{4+}$, showing 50% probability ellipsoids and atom-labeling scheme.

and atomic displacement parameters for **2** are given in Tables S3 and S4, respectively (supplementary material).

Physical Measurements. Magnetic susceptibility data were recorded over a temperature range of 10–300 K at a measuring field of 2.0 kOe with an SHE Corp. VTS-50 superconducting SQUID susceptometer interfaced to an IBM 9000 computer system. Calibration and operating procedures have been reported elsewhere.[20] Samples (elemental analyses obtained) weighing 30–50 mg were loaded into Delrin sample buckets. The sample measurements were corrected for the temperature dependence of the diamagnetism of the sample bucket. The temperature dependence of the molar magnetic susceptibility of the complexes, corrected for diamagnetism by using Pascal's constants,[20] can be found in Table S5 (supplementary material).

The temperature dependence data for $[Fe_2L(O_2CC_6H_4\text{-}4\text{-}F)_2](ClO_4)_3$ was analyzed by using the Heisenberg–Dirac–van Vleck spin Hamiltonian

$$H = -2JS_1 \cdot S_2 \qquad (1)$$

When the $S = {}^5/_2$ basis set for each interacting high-spin ferric ion is used, six spin-coupled energy levels result with coupled total spin quantum numbers $S_T = 0, 1, 2, 3, 4, 5$. The magnetic behavior that results from this distribution of energy levels may be obtained by the use of the van Vleck equation with the eigenvalues and eigenvectors of the spin coupling Hamiltonian; this gives rise to the equation

$$\chi = \frac{Ng^2\mu_B{}^2(2e^{2x} + 10e^{6x} + 28e^{12x} + 60e^{20x} + 110e^{30x})}{kT(1 + 3e^{2x} + 5e^{6x} + 7e^{12x} + 9e^{20x} + 11e^{30x})} \qquad (2)$$

where $x = J/kT$.[20]

The fits of the data to the van Vleck equation were greatly improved by correcting for the underlying temperature-independent paramagnetism of the Fe(III) ions as well as for the presence of a small amount of monomeric high-spin Fe(III) impurity. Thus, eq 2 was modified in the following manner:

$$\chi = (1 - P)\chi' + 2P\chi_c + 2(\mathrm{TIP}) \qquad (3)$$

where χ is the total calculated susceptibility, χ' is the spin-coupled susceptibility calculated from eq 2, P is the fraction of paramagnetic impurity, χ_c is the Curie law magnetic susceptibility of a high-spin ferric ion, and TIP is the underlying temperature-independent paramagnetism of the Fe(III) ions.

Infrared spectra were obtained on a Mattson Cygnus 25 FTIR spectrometer equipped with a HgCdTe detector. NMR spectra were run on an IBM AC-300 or a Nicolet NT-300 NMR spectrometer. Line shape analysis was performed by using software packages available on the NT-300 (NMCCAP) or the IBM-9000 (PEAK20) computers. The T_1 values for the various resonances of the complexes under study were obtained at 298 K by using a modified inversion-recovery pulse sequence: $(\pi/2)_x\text{-}\pi_y\text{-}(\pi/2)_x\text{-}\tau\text{-}(\pi/2)_x$–acquire. For the variable-temperature experiments, temperature calibration was accomplished by using methanol/HCl solutions.[21] The value for the antiferromagneic coupling, J, was extracted from the temperature dependence of the isotropic shifts as described previously.[22]

Table III. Atomic Parameters for the Non-Hydrogen Atoms of $[Fe_4O_2(L\text{-}Et)_2(OAc)_2]^{4+}$ (Cation of **2**)[a]

atom	x	y	z	B, Å^2
Fe1	0.3379 (2)	0.4542 (2)	0.4976 (2)	3.98 (7)
Fe2	0.5364 (2)	0.3451 (2)	0.4574 (2)	4.30 (7)
O12	0.4393 (8)	0.4010 (7)	0.4810 (9)	5.0 (3)
O	0.4078 (7)	0.5564 (7)	0.5994 (9)	4.4 (3)
O1E	0.3062 (8)	0.5122 (8)	0.3588 (9)	5.6 (4)
O2E	0.6185 (8)	0.3581 (7)	0.6082 (9)	5.4 (3)
N1	0.3463 (9)	0.4096 (9)	0.664 (1)	4.3 (4)
N2	0.476 (1)	0.3212 (9)	0.274 (1)	5.2 (4)
N1B	0.2559 (9)	0.3317 (9)	0.463 (1)	4.8 (4)
N3B	0.217 (1)	0.2115 (8)	0.522 (1)	5.9 (4)
N1A	0.2074 (9)	0.5009 (8)	0.529 (1)	4.5 (4)
N3A	0.1355 (9)	0.545 (1)	0.650 (1)	5.3 (4)
N1D	0.458 (1)	0.2221 (9)	0.438 (1)	5.9 (5)
N3D	0.349 (1)	0.130 (1)	0.334 (1)	6.7 (5)
N1C	0.638 (1)	0.2583 (9)	0.411 (1)	5.2 (4)
N3C	0.691 (1)	0.1881 (9)	0.285 (1)	7.3 (5)
C1	0.434 (1)	0.453 (1)	0.733 (1)	4.9 (5)*
C0	0.432 (1)	0.547 (1)	0.713 (1)	4.1 (4)*
C2	0.523 (1)	0.593 (1)	0.761 (1)	5.5 (5)*
C11B	0.347 (1)	0.313 (1)	0.653 (1)	4.8 (5)*
C2B	0.276 (1)	0.286 (1)	0.550 (1)	4.5 (4)*
C4B	0.160 (1)	0.214 (1)	0.418 (2)	6.4 (5)*
C9B	0.086 (2)	0.154 (1)	0.356 (2)	8.4 (6)*
C8B	0.046 (2)	0.176 (1)	0.262 (2)	8.7 (7)*
C7B	0.069 (2)	0.251 (1)	0.215 (2)	8.6 (7)*
C6B	0.140 (1)	0.309 (1)	0.279 (2)	6.1 (5)*
C5B	0.185 (1)	0.288 (1)	0.381 (1)	4.4 (4)*
C19	0.226 (2)	0.142 (2)	0.595 (2)	12.9 (9)*
C20	0.150 (2)	0.139 (2)	0.657 (2)	14 (1)*
C11A	0.267 (1)	0.436 (1)	0.703 (1)	5.5 (5)*
C2A	0.206 (1)	0.492 (1)	0.631 (1)	5.3 (5)*
C4A	0.093 (1)	0.583 (1)	0.557 (1)	4.9 (5)*
C9A	0.017 (1)	0.638 (1)	0.542 (2)	6.6 (6)*
C8A	−0.007 (1)	0.656 (1)	0.444 (2)	7.2 (6)*
C7A	0.025 (1)	0.634 (1)	0.357 (2)	6.9 (6)*
C6A	0.106 (1)	0.577 (1)	0.374 (2)	6.4 (5)*
C5A	0.137 (1)	0.553 (1)	0.479 (1)	5.2 (5)*
C29	0.122 (2)	0.555 (1)	0.755 (2)	7.6 (6)*
C30	0.174 (2)	0.634 (2)	0.820 (2)	11.4 (8)*
C11D	0.385 (1)	0.275 (1)	0.259 (1)	5.8 (5)*
C2D	0.394 (1)	0.212 (1)	0.339 (1)	5.9 (5)*
C4D	0.376 (2)	0.095 (1)	0.425 (2)	8.0 (6)*
C9D	0.359 (2)	0.015 (1)	0.472 (2)	8.2 (6)*
C8D	0.403 (1)	0.007 (1)	0.568 (2)	7.9 (6)*
C7D	0.468 (2)	0.061 (1)	0.643 (2)	8.6 (7)*
C6D	0.493 (2)	0.138 (1)	0.606 (2)	7.8 (6)*
C5D	0.446 (1)	0.153 (1)	0.499 (1)	6.0 (5)*
C39	0.272 (2)	0.093 (2)	0.235 (2)	15 (1)*
C40	0.314 (3)	0.034 (3)	0.158 (3)	19 (1)*
C11C	0.537 (1)	0.264 (1)	0.223 (2)	6.5 (5)*
C2C	0.617 (1)	0.241 (1)	0.305 (1)	6.0 (5)*
C4C	0.751 (2)	0.175 (1)	0.381 (2)	7.9 (6)*
C9C	0.833 (2)	0.123 (1)	0.405 (2)	8.4 (6)*
C8C	0.868 (2)	0.124 (2)	0.509 (2)	9.4 (7)*
C7C	0.848 (2)	0.159 (2)	0.596 (2)	10.1 (8)*
C6C	0.765 (1)	0.214 (1)	0.571 (2)	7.3 (6)*
C5C	0.723 (1)	0.217 (1)	0.468 (1)	5.5 (5)*
C49	0.686 (2)	0.147 (2)	0.171 (2)	13 (1)*
C50	0.632 (2)	0.054 (2)	0.137 (3)	16 (1)*
C7E	0.329 (1)	0.584 (1)	0.330 (1)	4.8 (5)*
C1E	0.287 (1)	0.599 (1)	0.211 (2)	6.4 (5)*

[a] Starred values denote atoms refined isotropically.

Results and Discussion

We have investigated the iron coordination chemistry of the ligand *N,N,N',N'*-tetrakis(2-benzimidazolylmethyl)-2-hydroxy-1,3-diaminopropane (L) to model active sites of iron–oxo proteins. We wanted to explore the potential of this binucleating ligand for assembling a (μ-alkoxo)bis(μ-carboxylato)diiron(III) unit with

(20) O'Connor, C. J. *Prog. Inorg. Chem.* **1979**, *29*, 204–283.
(21) Van Geet, A. L. *Anal. Chem.* **1970**, *6*, 679–680.
(22) Maroney, M. J.; Kurtz, D. M., Jr.; Nocek, J. M.; Pearce, L. L.; Que, L., Jr. *J. Am. Chem. Soc.* **1986**, *108*, 6871–6879.

Table IV. Bond Lengths (Å) and Bond Angles (deg) for the Cores in $[Fe_4O_2L_2(OBz)_2]^{4+}$ (Cation of **1**) and $[Fe_4O_2(L\text{-}Et)_2(OAc)_2]^{4+}$ (Cation of **2**)[a]

	1	2		1	2
Fe1–O12	1.789 (2)	1.796 (9)	Fe2–O12	1.798 (2)	1.791 (9)
Fe1–O	1.995 (2)	2.023 (8)	Fe2–O	2.018 (2)	1.987 (8)
Fe1–N1	2.306 (2)	2.25 (1)	Fe2–N2	2.271 (2)	2.26 (1)
Fe1–N1A	2.212 (2)	2.22 (1)	Fe2–N1C	2.187 (2)	2.23 (1)
Fe1–N1B	2.139 (2)	2.16 (1)	Fe2–N1D	2.177 (2)	2.16 (1)
Fe1–O1E	2.029 (2)	1.995 (9)	Fe2–O2E	2.014 (2)	1.964 (9)
Fe1···Fe2	3.539	3.488 (2)	Fe1···Fe2′(oxo)	3.580	3.586 (3)
O1E–C7E	1.260 (3)	1.26 (2)	O2E–C7E	1.266 (3)	1.24 (2)
O12–Fe1–N1A	173.47 (8)	170.9 (4)	O12–Fe2–N1C	171.01 (8)	169.9 (4)
O12–Fe1–N1B	89.93 (8)	90.7 (3)	O12–Fe2–N1D	88.50 (8)	90.7 (4)
O12–Fe1–O1E	96.05 (9)	96.1 (3)	O12–Fe2–O2E	97.69 (8)	97.8 (3)
O–Fe1–N1	78.08 (8)	77.6 (3)	O–Fe2–N2	77.89 (8)	76.3 (3)
O–Fe1–N1A	90.08 (8)	87.1 (3)	O–Fe2–N1C	86.85 (8)	89.7 (3)
O–Fe1–N1B	153.00 (9)	152.7 (4)	O–Fe2–N1D	152.60 (8)	153.1 (4)
O–Fe1–O1E	97.97 (8)	98.3 (3)	O–Fe2–O2E	96.57 (8)	97.8 (4)
N1–Fe1–N1A	76.56 (8)	77.1 (4)	N2–Fe2–N1C	77.79 (9)	77.1 (4)
N1–Fe1–N1B	74.92 (9)	75.6 (4)	N2–Fe2–N1D	75.06 (8)	77.1 (4)
N1–Fe1–O1E	162.63 (8)	165.7 (3)	N2–Fe2–O2E	165.35 (8)	165.4 (3)
N1A–Fe1–N1B	83.58 (8)	81.9 (3)	N1C–Fe2–N1D	83.30 (8)	80.5 (4)
N1A–Fe1–O1E	86.60 (8)	89.0 (4)	N1C–Fe2–O2E	88.44 (8)	89.7 (3)
N1B–Fe1–O1E	107.77 (9)	106.4 (4)	N1D–Fe2–O2E	108.61 (9)	106.4 (4)
Fe1–O12–Fe2	172.6 (1)	176.9 (5)	O1E–C7E–O2E	124.9 (3)	125 (1)
Fe1–O–Fe2	123.74 (9)	120.9 (4)	Fe2–O2E–C7E	138.1 (2)	136.6 (9)
Fe1–O1E–C7E	132.9 (2)	135.2 (9)			

[a] Estimated standard deviations in the least significant digit, given in parentheses, are derived from the inverse least-squares matrix. See text for qualifications on precision of bond parameters for **1**.

terminally coordinated imidazoles as a model for the hemerythrin active site. The ligands used include L and its 1-ethylbenzimidazole (L-Et) and 5,6-dimethyl (L-Me_2) derivatives; two types of complexes have been characterized, $[Fe_2L(O_2CR)_2]X_3$ and $[Fe_4O_2L_2(O_2CR)_2]X_4$. Precisely which complex is obtained is a function of the starting material and reaction conditions used. With $Fe(ClO_4)_3 \cdot xH_2O$, L or L-Et, and most aromatic carboxylates, $[Fe_2L(OBz)_2](ClO_4)_3$ or $[Fe_2(L\text{-}Et)(OBz)_2](ClO_4)_3$ is obtained directly from the reaction mixture. Using propionate instead of benzoate and metathesizing with $NaBPh_4$ results in the isolation of $[Fe_4O_2L_2(OPr)_2](BPh_4)_4$. With L-$Me_2$, only tetranuclear complexes are obtained. Tetranuclear complexes can also be obtained by the air oxidation of a solution of $Fe(OAc)_2$, L-Et, and $NaBF_4$ in ethanol and recrystallization of $[Fe_2L(OBz)_2](ClO_4)_3$ from CH_3CN/MeOH in the presence of sodium tosylate. Single crystals of $[Fe_4O_2L_2(OBz)_2](ClO_4)_2(OTs)_2$ (**1**) and $[Fe_4O_2(L\text{-}Et)_2(OAc)_2](BF_4)_4$ (**2**) were obtained and subjected to X-ray diffraction analysis.

Crystal Structures of $[Fe_4O_2L_2(OBz)_2](ClO_4)_2(OTs)_2$ and $[Fe_4O_2(L\text{-}Et)_2(OAc)_2](BF_4)_4$. **1** and **2** both crystallize in the space group $P\bar{1}$. A stereoview of the centrosymmetric cation for **1** is shown in Figure 1, while details of the connectivities within the tetranuclear core are more clearly revealed in Figure 2, where only the first coordination sphere about each iron center is shown. The tetracation of **2** exhibits a similar structure (Figure S1, supplementary material); small differences in the coordination geometries of **1** and **2** can be seen by inspection of Table IV. The iron centers, Fe1 and Fe2, are coordinated to one binucleating ligand; they are structurally similar but crystallographically unique. Each Fe atom has an N_3O_3 donor set in a distorted octahedron with the N-donors from the binucleating ligand (N1, N1A, N1B or N2, N1C, N1D) and the O-donors from a bridging oxide (O12), a bridging alkoxide (O), and a bridging bidentate carboxylate (O1E (O2E)).

The two pairs of iron atoms are arranged in a nearly tetragonal array with O–Fe1–O12 and O–Fe2–O12 angles in the range of 95–99°. For **1**, the Fe–Fe separations are 3.54 and 3.58 Å across the alkoxo and the oxo bridges, respectively, while for **2**, the corresponding distances are 3.49 and 3.59 Å, respectively. The Fe–O(oxo) bonds, which average 1.794 (4) Å, fall in the middle of the range for such bonds (1.76–1.82 Å).[23] The oxo bridges are nearly linear with Fe–O–Fe angles of 172.6 (1) and 176.9 (5)° for **1** and **2**, respectively; these values lie at the high end of the range for other oxo-bridged complexes (116–180°).[9-11,23]

The Fe–O(alkoxo) bonds average 2.006 (17) Å; other Fe–O distances in $Fe_2(\mu\text{-}OR)$ units for comparison include [Fe(SALPA)(SALPAH)]$_2$ (1.93, 1.97, 1.99, and 2.00 Å),[24] $[Fe_2((sal)_3trien)(OMe)Cl_2]$ (1.95 and 2.00 Å),[25] and $[Fe_4O_2(HPTAz)_2(CO_3)_2]^{6-}$ (2.040 and 2.066 Å).[13a] The Fe–OR–Fe angles of 123.7 (1) and 120.9 (4)° are smaller than that found in $[Fe_4O_2(HPTA)_2(CO_3)_2]^{6-}$ (132.3°)[13a] and reflects the presence of the carboxylate bridge, which requires a smaller Fe1–Fe2 separation. The bridging carboxylate is symmetrically bridged between Fe1 and Fe2, with Fe–O bond lengths comparable to those found for μ-acetato complexes such as $[(HB(pz)_3Fe)_2O(OAc)_2]$ (2.043 Å)[9] and $[(HB(pz)_3Fe)_2OH(OAc)_2]^+$ (1.999 Å).[26]

The Fe–N(amine) bonds at 2.26–2.31 Å are in the upper end of the range found for corresponding Fe–N bonds in other tripodal ligand complexes (e.g.: $[Fe(NTA)DBC]^{2-}$, 2.224 Å;[27] [Fe(HEDTA)]$_2O^{2-}$, 2.25 Å;[28] $[Fe_4(5\text{-}Me\text{-}HXTA)_2O_2(OH)_2]^{4-}$, 2.233 Å;[14] Li[Fe(EDTA)H_2O], 2.325 Å;[29] $[N_5FeOFeCl_3]^+$, 2.284 and 2.358 Å[30]). The Fe–N(benzimidazole) bonds average 2.185 Å and are longer than those found for $[N_5FeOFeCl_3]^+$ (2.094 Å)[30] and the Fe–N(imidazole) bonds in $[Fe_3O(TIEO)_2(OBz)_2Cl_3]$ (2.146 Å)[12] and $[Fe(salhis)_2]PF_6$ (2.147 Å).[31] Those bonds trans to the bridging oxo group are significantly longer than those which are cis.

The structural parameters for the binucleating ligand are as expected and will not be discussed further. However, a dominant feature of the assembly of the tetranuclear cation is the pairwise stacking of the benzimidazole groups, involving π–π interactions (Figure 1 and S1). One pair is formed between benzimidazole

(23) Murray, K. S. *Coord. Chem. Rev.* **1974**, *12*, 1–35.
(24) Bertrand, J. A.; Eller, P. G. *Inorg. Chem.* **1974**, *13*, 927–934.
(25) Chiari, B.; Piovesana, O.; Tarantelli, T.; Zanazzi, P. F. *Inorg. Chem.* **1982**, *21*, 2444–2448.
(26) Armstrong, W. H.; Lippard, S. J. *J. Am. Chem. Soc.* **1984**, *106*, 4632–4633.
(27) Que, L., Jr.; Kolanczyk, R. C.; White, L. S. *J. Am. Chem. Soc.* **1987**, *109*, 5373–5380.
(28) Lippard, S. J.; Schugar, H. J.; Walling, C. *Inorg. Chem.* **1967**, *6*, 1825–1831.
(29) Hamor, M. J.; Hamor, T. A.; Hoard, J. L. *Inorg. Chem.* **1964**, *3*, 34–43.
(30) Gomez-Romero, P.; DeFotis, G. C.; Jameson, G. B. *J. Am. Chem. Soc.* **1986**, *108*, 851–853.
(31) Davis, J. C.; Kung, W.-J.; Averill, B. A. *Inorg. Chem.* **1986**, *25*, 394–396.

Table V. Comparison of Core Structural Parameters of **1**, **2**, and $[Fe_4O_2(HPTA)_2(CO_3)_2]^{6-}$

param	av (**1** and **2**)[a]	$[Fe_4O_2(HPTA)_2(CO_3)_2]^{6-}$ [a,b]
Fe–O(oxo), Å	1.794 (4)	1.829 (4)
Fe–O(alkoxo), Å	2.01 (2)	2.05 (1)
Fe–O(O_2CX), Å	2.00 (3)	1.992 (4)
Fe–O(oxo)–Fe, deg	175 (3)	136.4 (3)
Fe–O(alkoxo)–Fe, deg	122 (2)	132.3 (2)
Fe1···Fe2 (alkoxo), Å	3.51 (4)	3.755
Fe1···Fe2 (oxo), Å	3.583 (4)	3.397

[a] Esd value in parentheses is the larger of that for an individual bond parameter or that calculated from the scatter of values about their mean. [b] Reference 14a.

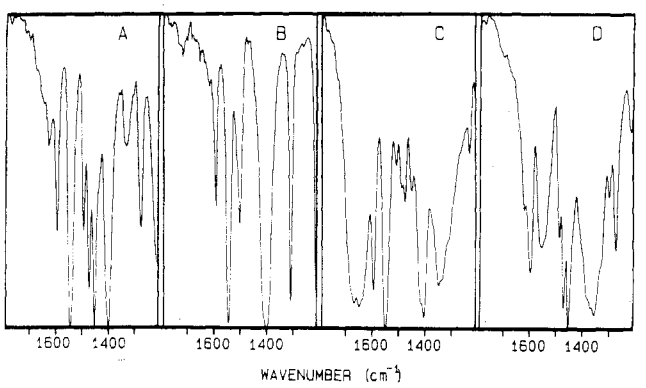

Figure 3. Comparison of FTIR spectra (1200–1700 cm^{-1}): (A) $[Fe_4O_2L_2(OBz)_2](ClO_4)_2(OTs)_2$; (B) $[(HB(pz)_3Fe)_2O(OBz)_2]$; (C) $(Me_4N)[Fe_2(5\text{-Me-HXTA})(OBz)_2]$; (D) $[Fe_2L(OBz)_2](ClO_4)_3$.

moieties of the same ligand molecule—that is, between benzimidazole groups of the $Fe_2L(OBz)$ or $Fe_2(L\text{-Et})(OAc)$ unit. The second pair is formed upon linking the binuclear units via the μ-oxo groups. Such interactions may contribute to the stability of the tetranuclear complexes.

Structural parameters for $[Fe_4O_2L_2(O_2CR)_2]^{4+}$ and $[Fe_4O_2(HPTA)_2(CO_3)_2]^{6-}$, tetranuclear complexes of related ligands, are compared in Table V. L shares the same binucleating framework as HPTA with the pendant functionalities being benzimidazoles instead of carboxylates. Both complexes are assembled from two binucleating ligands, two carboxylate bridges, and two oxo bridges, except that the metal–ligand connectivities are permuted. $[Fe_4O_2(HPTA)_2(CO_3)_2]^{6-}$ consists of two Fe_2HPTA units linked by oxo and carbonato bridges, while $[Fe_4O_2L_2(O_2CR)_2]^{4+}$ consists of two $Fe_2L(\mu\text{-}O_2CR)$ units bridged by oxo groups. Thus, the carbonato bridge in the former connects iron centers of different Fe_2HPTA units, while the carboxylates in the latter complexes connect iron centers within the same Fe_2L unit. The diffeences in bridging arrangements are reflected in the Fe–Fe distances and Fe–O–Fe angles, with the carboxylato-bridged diiron unit exhibiting the shorter distance and the smaller angle relative to the corresponding diiron unit in the other complex. In addition, the pendant benzimidazole ligands are cis to one another in $[Fe_4O_2L_2(O_2CR)_2]^{4+}$, whereas in $[Fe_4O_2(HPTA)_2(CO_3)_2]^{6-}$ the corresponding carboxylates are trans. Overall, the Fe–O(oxo) and Fe–O(alkoxo) bonds in $[Fe_4O_2L_2(O_2CR)_2]^{4+}$ are shorter than those in $[Fe_4O_2(HPTA)_2(CO_3)_2]^{6-}$, while the remaining metal–ligand bonds are longer. The rationale for these structural differences is unclear. The shorter Fe–O(bridge) bonds in $[Fe_4O_2L_2(O_2CR)_2]^{4+}$ undoubtedly give rise to the stronger antiferromagnetic coupling observed for this complex (vide infra).

Physical Properties of $[Fe_4O_2L_2(OBz)_2]X_4$. Physical measurements on $[Fe_4O_2L_2(O_2CR)_2]^{4+}$ complexes support the crystallographic results. Their IR spectra show sharp features near 745 and 825 cm^{-1}, characteristic of ortho-disubstituted benzene (benzimidazole) and $\nu_{as}(FeOFe)$[9,23] modes, respectively. The 1300–1700-cm^{-1} region for $[Fe_4O_2L_2(OBz)_2]^{4+}$ is shown in Figure 3A and compared with those of $[(HB(pz)_3Fe)_2O(OBz)_2]$[9] (Figure 3B) and $(Me_4N)[Fe_2(5\text{-Me-HXTA})(OBz)_2]$[32] (Figure 3C); the

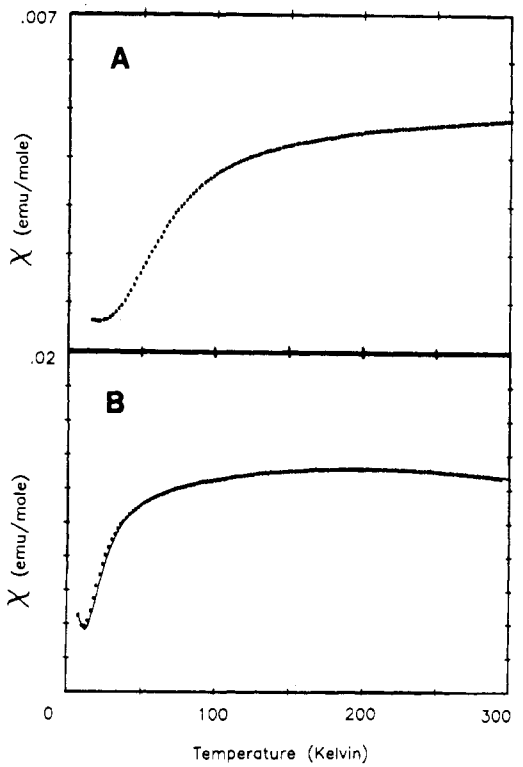

Figure 4. Variable-temperature magnetic susceptibility data: (A) $[Fe_4O_2L_2(OBz)_2](ClO_4)_2(OTs)_2$; (B) $[Fe_2L(O_2CC_6H_4\text{-}4\text{-}F)_2](ClO_4)_3$.

bridging bidentate benzoate coordination is clearly indicated by prominent $\nu_s(COO)$ and $\nu_{as}(COO)$ features at 1400–1410 and 1540–1550 cm^{-1}, respectively. Similar prominent features are found at these values in the spectra of other complexes with 1,3-μ-carboxylato groups.[33,34]

Solid-state magnetic susceptibility measurements on $[Fe_4O_2L_2(OBz)_2](ClO_4)_2(OTs)_2$ and $[Fe_4O_2(L\text{-}Me_2)_2(OBz)_2](ClO_4)_4$ indicate the presence of strong antiferromagnetic coupling, with room-temperature μ_{eff} values of 1.7 and 1.9 μ_B/Fe, respectively. These values are smaller than that observed for $[Fe_4O_2(HPTA)_2(CO_3)_2]^{6-}$ (μ_{eff} = 2.4 μ_B/Fe, J = −63.4 cm^{-1}, J' = −11.2 cm^{-1})[13a] and reflect the shorter Fe–O(bridge) bond lengths in $[Fe_4O_2L_2(OBz)_2]^{4+}$, which undoubtedly promote stronger coupling between the metal centers.[35] We have also obtained variable-temperature data (shown for $[Fe_4O_2L_2(OBz)_2](ClO_4)_2(OTs)_2$ in Figure 4A), but their analysis has been hindered by the large amount of cross coupling between pairs of Fe_2O units via the alkoxo bridge. We are able to get excellent agreement between theory and experiment using the binuclear model corrected with the molecular field approximation[20] (g = 2.0; J = −83 cm^{-1}, zJ' = −107 cm^{-1}, TIP = 0.000 68 emu/mol). However, the molecular field approximation is only valid for $|zJ'| \ll |J|$; i.e., $|zJ'|$ is no more than about 10% of $|J|$. Since the fit results in the *inter* binuclear coupling (zJ') being greater than the *intra* binuclear coupling, it is necessary to solve the magnetic susceptibility equation exactly using the complete Hamiltonian and the four-spin product basis set. The solution of this problem is nontrivial (1296 wave functions) and will be the subject of a future report.

The NMR spectra of the tetranuclear complexes indicate that the tetranuclear structure is maintained in solution (Figure 5).

(32) Murch, B. P.; Bradley, F. C.; Que, L., Jr. *J. Am. Chem. Soc.* **1986**, *108*, 5027–5028. Borovik, A. S., unpublished observations.
(33) Nakamoto, K. *Infrared and Raman Spectra of Inorganic and Coordination Compounds*, 3rd ed.; Wiley: New York, 1978; p 232. Mehrotra, R. C.; Bohra, R. *Metal Carboxylates*; Academic: New York, 1983; p 53.
(34) Sheats, J. E.; Czernuszewicz, R. S.; Dismukes, G. C.; Rheingold, A. L.; Petrouleas, V.; Stubbe, J.; Armstrong, W. H.; Beer, R. H.; Lippard, S. J. *J. Am. Chem. Soc.* **1987**, *109*, 1435–1444.
(35) Gorun, S. M.; Lippard, S. J. *Recl. Trav. Chim. Pays-Bas* **1987**, *106*, 417.

Table VI. NMR Data (ppm) for Complexes[a] of L and L-Me_2

assignt	A[b]	B[b]	C[b]	D	E	F	G	H	I	J
	45.6	45.6 [~1]	45.8 [~1]	45.5	45.0	45.1				
	31.4	30.7 [~1]	31.2 [~1]	31.1	30.6	30.7				
	24.8	24.4 [~1]	24.5 [~1]	24.7	25.3	25.2				
Bzim NH	15.9 [3.8]	16.8 [3.3]	16.8 [2.9]	15.9	16.0	17.5	49.6	49.6	49.6	50
Bzim NH	13.8 [4.4]	14.8 [4.0]	14.8 [3.3]	14.0	13.9	15.6	45.3	45.3	45.3	45
	NO[c]	12.9 [~1]	12.9 [~1]	NO	NO	NO				
Bzim C7H	12.3 [12.3]	12.2 [13.6]	12.2 [13.0]	12.5	12.4	12.1	34.0	34.0	34.0	34.0
Bzim C7H	9.5 [12.3]	9.4 [11.7]	9.4 [12.0]	9.7	9.7	9.4				
OBz *m*-H		9.4 [11.7]	9.1 [9.9]	9.3			10.7	10.5		10.6
OBz *p*-H		7.9 [18.3]					6.1		6.6	
							7.9	8.1	8	8
							7.5	7.3	7	7
	NO	7.5 [<1]	7.5 [<1]	NO	NO	7.5				
Bzim C(5 or 6)H	7.4 [19.1]			7.6	7.5					
Bzim C(5 or 6)H	6.9 [13.9]			7.1	7.0					
Bzim C(5 or 6)H	6.1 [16.2]			6.4	6.4					
Bzim C6Me		2.7 [50]	2.7 [38]			2.7				
Bzim C5Me		2.3 [25]	2.3 [20]			2.3				
Bzim C6Me		2.1 [40]	2.1 [30]			2.1				
Bzim C5Me		1.6 [11.8]	1.6 [12.5]			1.6				
OPr-CH_2					8					
$(O_2CC_6H_4)$-4-CH_3				3.4						4.6
OAc-CH_3						10.9				

[a] A, D, and E are $[Fe_4O_2L_2(O_2C\text{-}R)_2]^{4+}$ where R = $-C_6D_5$, $-C_6H_5$-4-CH_3, and $-CH_2CH_3$, respectively; B, C, and F are $[Fe_4O_2(L\text{-}Me_2)_2(O_2C\text{-}R)_2]^{4+}$ where R = $-C_6H_5$, $-C_6H_4$-4F, $-CH_3$, respectively; G, H, I, and J are $[Fe_2L(O_2C\text{-}R)_2]^{3+}$ where R = $-C_6H_5$, $-C_6H_4$-4-F, $-C_6H_3$-3,5-Cl_2, and $-C_6H_5$-4-CH_3, respectively. [b] Numbers in brackets are T_1 values of the associated proton in units of milliseconds. [c] Not observable due to interfering resonances.

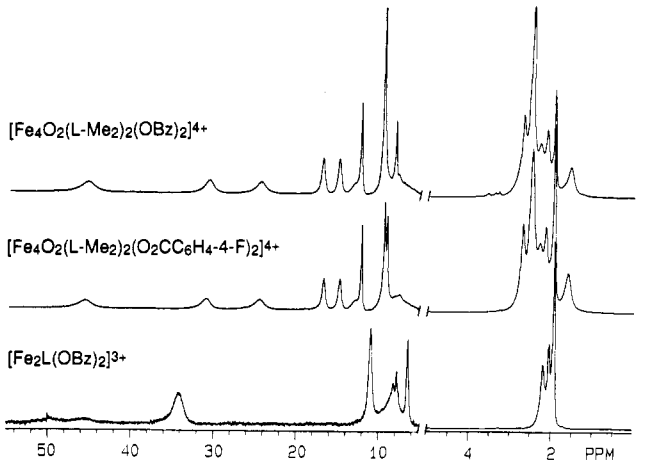

Figure 5. Comparison of NMR spectra for tetranuclear complexes, $[Fe_4O_2(L\text{-}Me_2)_2(OBz)_2]^{4+}$ and $[Fe_4O_2(L\text{-}Me_2)_2(O_2CC_6H_4\text{-}4\text{-}F)_2]^{4+}$, and a binuclear complex, $[Fe_2L(OBz)_2]^{3+}$. Samples (ca. 10 mg) were dissolved in 0.38 mL of CD_3CN/0.02 mL DMSO d_6, and spectra were recorded at 300 K. Note that there is a change of scale on both the x an y axes for the 0–5 ppm region.

Relatively sharp lines and small isotropic shifts are observed because of the strong antiferromagnetic coupling between the iron centers. The chemical shifts of the features observed for the various complexes are listed in Table VI, together with proposed assignments that have been derived from a combination of atom substitution experiments and T_1 measurements. Two features in the 14–17 ppm region disappear when methanol-d_4 is added to the CD_3CN solution and are thus assigned to the benzimidazole N–H protons. The presence of the two peaks reflects the differences in metal–ligand bonding between the benzimidazole trans to the alkoxo bridge and that trans to the oxo bridge. The observed shifts are significantly smaller than those predicted from high-spin ferric imidazole complexes (ca. 100 ppm)[36] and reflect the strong antiferromagnetic coupling between the iron centers. The strong coupling ($J \approx -100$ cm^{-1}) reduces the room-temperature magnetic susceptibility of the complex to about 10% of that expected for a mononuclear high-spin ferric complex; this reduction is reflected in the isotropic shifts of the N–H protons. The region where the N–H resonances are found is also where histidine N–H resonances have been observed in methemerythrin[22] and ribonucleotide reductase.[37]

The broad features at ca. 8, 12, 25, 32, and 45 ppm exhibit the shortest T_1 values and are thus assigned to protons nearest the metal center,[38] such as the aliphatic protons of the binucleating ligand, the benzoate ortho protons, and the benzimidazole C4H protons. The benzoate meta and para protons are conveniently assigned by using substituted benzoates, as are the benzimidazole C5H and C6H protons by a comparison of L and L-Me_2 complexes. These exhibit relatively long T_1 values (~10–20 ms). Two other features at ca. 12 and 9.5 ppm exhibit T_1 values similar to that of the benzoate meta protons and are associated with the C7H protons of the inequivalent benzimidazoles.

Structure and Properties of $[Fe_2L(OBz)_2]X_3$. Treatment of L with $Fe(ClO_4)_3$, benzoic acid, and triethylamine in a 1:2:2:2 ratio in methanol yields microcrystalline material that is analyzed as $[Fe_2L(OBz)_2](ClO_4)_3$. The use of halogenated benzoic acids in the synthesis also results in complexes with the same stoichiometry; however, we have been unable to isolate the analogous complex with aliphatic carboxylates.

Spectroscopic characterization of these complexes has included magnetic susceptibility, infrared, and NMR studies. The variable-temperature magnetic susceptibility data on $[Fe_2L(O_2CC_6H_4\text{-}4\text{-}F)_2](ClO_4)_3$ plotted in Figure 4B indicates the presence of modest antiferromagnetic coupling. The coupling presumably reflects the interaction of the ferric ions via the alkoxo group. Excellent fits of the data are obtained for $J = -26$ cm^{-1}, $g = 2.0$, TIP = 0.000 059, and 0.75% mononuclear high-spin ferric impurity. This J value is somewhat larger than those estimated for complexes with $Fe_2(\mu\text{-}OR)_2$ units (−17 cm^{-1}), such as $[Fe(SALPA)Cl]_2$[39] and $[Fe(SALPA)(SALPAH)]_2$.[24] Similarly, the J value for $[(HB(pz)_3Fe)_2OH(OAc)_2]^+$ ($J = -17$ cm^{-1}),[26] which contains an $Fe_2(\mu\text{-}OH)$ unit, is larger than those observed for complexes with $Fe_2(\mu\text{-}OH)_2$ units (J = ca. −10 cm^{-1}).[40]

(36) Lauffer, R. B.; Anatanaitis, B. C.; Aisen, P.; Que, L., Jr. *J. Biol. Chem.* **1983**, *258*, 14212–14218.
(37) Sahlin, M.; Ehrenberg, A.; Graslünd, A.; Sjöberg, B.-M. *J. Biol. Chem.* **1986**, *261*, 2778–2780.
(38) Bertini, I.; Luchinat, C. *NMR of Paramagnetic Molecules in Biological Systems*; Benjamin Cummins: Menlo Park, CA, 1986.
(39) Bertrand, J. A.; Breece, J. L.; Eller, P. G. *Inorg. Chem.* **1974**, *13*, 125–131.
(40) Ou, C. C.; Lalancette, R. A.; Potenza, J. A.; Schugar, H. J. *J. Am. Chem. Soc.* **1978**, *100*, 2053–2057.

Table VII. Chemical Shifts of Benzoate Meta Protons for Various Complexes

complex	δ	δ_{iso}[a]	J, cm^{-1}	% of $\chi(Fe^{III})$[b]	δ-(uncoupled)
$[(HB(pz)_3Fe)_2O(OBz)_2]$[c]	8.7	1.3	−120	8	16.2
$[Fe_2(5\text{-Me-HXTA})(OBz)_2]^-$[d]	18	10.6	−10	72	14.7
$[Fe_4O_2L_2(OBz)_2]^{4+}$	9.4	2.0	~−100	~10	20
$[Fe_2L(OBz)_2]^{3+}$	10.7	3.3	−20	51	6.5
Fe(TTPPP)OBz[e]	13.5	6.1	0	100	6.1
Fe(salen)OBz	11.9	4.5	0	100	4.5

[a] Diamagnetic shift of benzoate *m*-H set at 7.4 ppm. [b] $\chi(J)/\chi(J = 0)$ calculated from eq 2. [c] Reference 9. [d] Reference 32. [e] Reference 41.

In agreement with the magnetic susceptibility studies, the NMR spectra of the binuclear complexes show features that are broadened and significantly more paramagnetically shifted relative to the corresponding features of the tetranuclear complexes (Figure 5, Table VI). Since the contact shift of a particular ligand proton is proportional to the magnetic susceptibility of the complex,[38] the binuclear complexes are calculated to exhibit shifts 5-fold larger than those for the tetranuclear complexes. For $J = -26$ cm^{-1}, eq 2 yields a value of χ_M/Fe which is 42% of that calculated for $J = 0$, while the tetranuclear complexes exhibit room-temperature susceptibilities 9–10% of that expected for an uncoupled high-spin ferric center.

The NH siganls are found at 46 and 50 ppm; these disappear when methanol-d_4 is added to the solvent. These features are also absent in the spectrum of $[Fe_2(L\text{-Et})(OBz)_2](ClO_4)_3$. The isotropic shifts of these protons are at slightly less than half the value expected for a mononuclear ferric imidazole complex,[36] consistent with the J value obtained from solid-state susceptibility measurements. When compared to the NH shifts of the tetranuclear complexes (and a diamagnetic position of 8 ppm assumed for the NH proton), the NH shifts of the binuclear complexes do exhibit the expected 5-fold larger magnitude.

The feature at ca. 34 ppm for the binuclear complex presumably corresponds to the feature at 12 ppm in the tetranuclear complex and is associated with the benzimidazole C7H protons. Its temperature dependence was obtained because of its large shift and relative sharpness (Figure S3); the data fit well to a curve simulating $J = -19 \pm 2$ cm^{-1}, in good agreement with the solid-state data. As with the N–H protons, the ratio of isotropic shifts for the binuclear and tetranuclear complexes is about 5 (assuming a diamagnetic position of 7 ppm).

The peak at 11 ppm is associated with the benzoate meta protons by comparison with the 3,5-dichlorobenzoate complex. In contrast to the case for the NH and C7H protons, the isotropic shift of the benzoate meta protons is less than twice that observed for the benzoate meta protons of the corresponding tetranuclear complex (assuming a diamagnetic position of 7.4 ppm). Table VII complexes the isotropic shifts of a series of benzoate complexes after correcting for the presence of antiferromagnetic coupling. The benzoate meta protons in the tetranuclear complex, **1**, exhibit a shift similar to those of other complexes with bridging benzoates; however, the corresponding protons in the binuclear complex exhibit a significantly smaller shift, one that more closely matches those of the mononuclear Fe(TTPPP)OBz[41] and Fe(salen)OBz. The differences in shift indicate that a smaller amount of unpaired spin density is delocalized onto the binuclear carboxylate, suggesting that there are differences in the iron–carboxylate interaction in the binuclear and tetranuclear complexes. The methyl isotropic shifts in iron(III) acetate complexes have been shown to be sensitive to the acetate coordination mode as well.[42]

The infrared spectra of the binuclear and tetranuclear complexes also show differences in the mode of carboxylate coordination (Figure 3, Table VIII). The strong features at ca. 1400 and 1550 cm^{-1} for the tetranuclear complexes assigned to the ν_s(COO) and ν_{as}(COO) modes, respectively, are typical of complexes with a bridging bidentate carboxylate.[33] These broaden and move to 1358 and 1556 cm^{-1} in the spectrum of $[Fe_2L(OBz)_2](ClO_4)_3$. The energy difference between the ν_s(COO) and ν_{as}(COO) modes is diagnostic of the geometry of carboxylate coordination (Table VIII).[33] Monodentate coordination is associated with an energy difference of 220–460 cm^{-1} and with the higher energy mode at greater than 1600 cm^{-1} as occurs for Fe(TTPPP)OBz.[41] Bidentate nonbridging coordination is associated with an energy difference of 40–80 cm^{-1}, while for bridging bidentate coordination the difference is in the range of 140–170 cm^{-1}.[33] For $[Fe_2L(OBz)_2]^{3+}$, the difference is 198 cm^{-1}, intermediate between the ranges expected for bridging bidentate carboxylates and for monodentate carboxylates. Thus, we propose that the benzoates in $[Fe_2L(OBz)_2]^{3+}$ both bridge the iron centers, but in a significantly asymmetric manner. The asymmetric bridging would have to be more pronounced than that found for $[Fe_2(5\text{-Me-HXTA})(OAc)_2]^-$ (Δr for Fe–O(carboxylate) = 0.08 Å), since the correspondence benzoate complex exhibits COO stretching features typical of a bridging bidentate carboxylate. Such a coordination mode may also be expected to result in the delocalization of less unpaired spin density from the paramagnetic center, as is the case with monodentate carboxylates.

Table VIII. Comparison of Carboxylate Stretching Modes

	ν_{as}, cm^{-1}	ν_s, cm^{-1}	$\Delta\nu$, cm^{-1}	ref
bidentate, bridging	1580	1410–1440	140–170	33
bidentate, nonbridging	1510–1550	1450–1470	40–80	33
monodentate	1600–1725	1267–1380	220–460	33
free acetate	1414	1578	164	33
$[Fe_4L_2(OBz)_2]^{4+}$	1544	1400	144	*a*
$[Fe_4(L\text{-Et})_2(OAc)_2]^{4+}$	1545	1410	135	*a*
$[(HB(pz)_3Fe)_2O(OBz)_2]$	1544	1401	143	9, *a*
$[Fe_2(5\text{-Me-HXTA})(OBz)_2]^-$	1549	1404	145	32
$[Fe_2L(OBz)_2]^{3+}$	1556	1358	198	*a*
Fe(TTPPP)OBz	1656	1298	358	41

[a] This work.

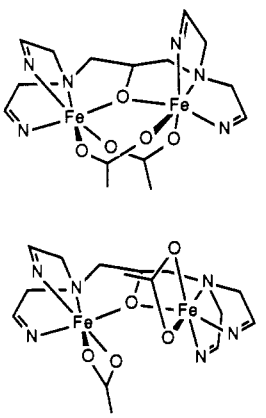

Figure 6. Possible structures for $[Fe_2L(OBz)_2]^{3+}$: (top) triply bridged bis(μ-1,3-carboxylato)geometry (the alkoxo C–O bond lies in an approximate mirror plane perpendicular to the page); (bottom) singly bridged geometry with bidentate nonbridging carboxylates (an approximate 2-fold axis is coincident with the alkoxo C–O bond).

In Figure 6, we show a representation for the (μ-alkoxo)bis(μ-carboxylato) structure as well as one for a nonbridging bidentate coordination mode. Meridional conformations such as those found for $[Fe_2(5\text{-Me-HXTA})OH(H_2O)_2]$ and $[Fe_4O_2(HPTA)(CO_3)_2]^{6-}$ are also possible for L or L-Et. Note that the conformation of L or L-Et seen in the tetranuclear complexes would lead to steric interference of the carboxylate groups if each were to coordinate in a nonbridging bidentate manner in the binuclear complex. The binucleating ligands in this study comprise two N_3 moieties—that may each cap the face of an octahedron—linked by a three-carbon 2-hydroxypropyl chain. This chain places stereochemical re-

(41) Watanabe, Y.; Groves, J. T. *Inorg. Chem.* **1987**, *26*, 785–786. Watanabe, Y.; Groves, J. T., personal communication.
(42) Arafa, I. M.; Goff, H. M.; David. S. S.; Murch, B. P.; Que, L., Jr. *Inorg. Chem.* **1987**, *26*, 2779–2784.

Table IX. Dihedral Angles between N_3 Moieties in Binuclear Complexes

complex	dihedral angle, deg	ref
Triply Bridged, Two Bridging Carboxylates		
$[(HB(pz)_3Fe)_2O(OAc)_2]$	49.4	9
$[(HB(pz)_3Fe)_2O(O_2CH)_2]$	49.2	9
$[(HB(pz)_3Fe)_2OH(OAc)_2]ClO_4$	55.3	26
$[(HB(pz)_3Fe)_2O(O_2P(OR)_2)_2]$[a]	56.5	43
$[(N3Fe)_2O(OAc)_2](ClO_4)_2 \cdot EtOH$	42.9 (3)	12
$[(N3Fe)_2O(OBz)_2](ClO_4)_2 \cdot (Et_3NHClO_4) \cdot 2EtOH$	42.1 (2)	12
$[(N3Fe)_2O(OBz)_2](ClO_4)_2 \cdot 0.5Et_3NHClO_4 \cdot EtOH$	35.8 (2)	12
metazidohemerythrin[b]	62–66	6
$[Fe_2(LXy)(OBz)_2](BF_4)_2 \cdot xCH_3CN$	48.3 (10)	44
$Me_4N[Fe_2(5\text{-Me-HXTA})(OAc)_2]$[c]	42.8	32
$(C_4H_{10}N)_4[Fe_4O_2(OH)_2(5\text{-Me-HXTA})_2]$[c,d]	62.3	14
Doubly Bridged, One Bridging Carboxylate		
$[Fe_4O_2L_2(OBz)_2](ClO_4)_2(OTs)_2$	89.9	e
$[Fe_4O_2(L\text{-Et})_2(OAc)_2](BF_4)_4 \cdot 8H_2O$	87.4 (5)	e

[a] Bridging phosphate diesters instead of carboxylates. [b] The first N_3 plane is defined by the three coordinated imidazole nitrogen atoms on one Fe, while the second N_3 plane is defined by the two coordinated imidazole nitrogen atoms and the coordinated nitrogen atom of the azide on the other Fe. [c] The N_3 planes are replaced by NO_2 planes, where O refers to the coordinated carboxylate oxygen atoms of 5-Me-HXTA. [d] Bridging hydroxide instead of bridging carboxylate groups. [e] This work.

strictions on the juxtaposition of the two octahedra. A convenient measure of this restriction is the dihedral angle between the planes defined by the three ligating atoms of each N_3 moiety. These planes are drawn in Figure 2, and values of the dihedral angle for a variety of multiply bridged iron complexes of bioinorganic interest are tabulated in Table IX. Considerable conformational variability is seen in unconstrained triply bridged diiron systems that are models for metazidohemerythrin. Thus, for these bisoctahedral complexes, such as $[(HB(pz)_3Fe)_2O(OAc)_2]$,[9] $[(HB(pz)_3Fe)_2OH(OAc)_2]^+$,[26] $[(HB(pz)_3Fe)_2O(O_2P(OR)_2)_2]$,[43] and $[(N3Fe)_2O(O_2CR)_2]^{2+}$ (R = CH_3, Ph),[12] the dihedral angles lie in the 35–55° range. For the five-carbon 2-hydroxy-1,3-xylylene-linked binuclear iron complexes such as $[Fe_2(5\text{-Me-HXTA})(OAc)_2]^-$[32] and $[Fe_2(LXy)(OBz)_2]^{2+}$,[44] similar dihedral angles are found. On the other hand, in the doubly bridged diiron centers of the tetranuclear complexes of L and L-Et, where there is only a three-carbon bridge, the angles observed are close to 90°. To accommodate a second bridging carboxylate, as proposed for $[Fe_2L(OBz)_2]^{3+}$, requires twisting the septadentate ligand to change this dihedral angle. This may be achieved while still maintaining approximately gauche conformations in the propylene bridge, as illustrated in Figure 6. However, the resulting strain may cause the carboxylates to adopt a highly unsymmetrical bridging mode in the binuclear complexes.

Binuclear vs Tetranuclear. The conditions that determine the nuclearity of the complexes of this binucleating ligand are unclear. For L and L-Et, microcrystalline binuclear complexes are obtained initially with most aromatic carboxylates; however, tetranuclear complexes are obtained with acetate, propionate, and *p*-toluate. For L-Me_2, only tetranuclear complexes have been obtained in the synthetic experiments, and the associated carboxylate can be either aromatic or aliphatic. When the binuclear complexes are dissolved in acetonitrile, they slowly convert to the corresponding tetranuclear complexes over a period of 2 weeks. The conversion is most readily monitored by NMR spectroscopy, which shows the gradual replacement of the broad features of the binuclear complex with the much sharper features of the tetranuclear complex. The driving force for the formation of the tetranuclear complex may arise from the Lewis acidity and oxophilicity of the iron center and the $\pi-\pi$ interactions between the benzimidazole groups. Formation of the μ-oxo bridge requires water or hydroxide ion, which is usually available adventitiously. The conversion of binuclear to tetranuclear complex can in principle be conceived as

$$2[Fe_2L(OBz)_2]^{3+} + 2OH^- \rightarrow [Fe_4O_2L_2(OBz)_2]^{4+} + 2\ BzOH$$

Model-building studies of the binuclear complex suggest that the conversion is likely to require a substantial change in ligand conformation, entailing a substantial activation barrier. The NMR observations are consistent with such a slow conversion.

Acknowledgment. This work has been supported by the National Institutes of Health (Grant GM-33162, L.Q.; Grant DK-37702, G.B.J.) and the E. G. Schleider Educational Foundation (C.J.O.). We thank Bridget A. Brennan for experimental assistance.

Supplementary Material Available: Tables S1–S4, listing H atom and solvent atom parameters and temperature factors, respectively, for **1** and **2**, Table S5, listing magnetic susceptibility data on $[Fe_4O_2L_2(OBz)_2](ClO_4)_2(OTs)_2 \cdot CH_3OH \cdot 3H_2O$, $[Fe_4O_2(L\text{-}Me_2)_2(OBz)_2](ClO_4)_4 \cdot 3H_2O$, and $[Fe_2L(O_2CC_6H_4\text{-}4\text{-}F)_2](ClO_4)_3$, Figure S1, showing the cation of **2**, Figure S2, showing the crystallographic numbering scheme for the ligand, and Figure S3, showing the temperature dependence of the C7H isotropic shift for $[Fe_2L(OBz)_2]^{3+}$ in CD_3CN (17 pages); listings of observed and calculated structure factors for **1** and **2** (65 pages). Ordering information is given on any current masthead page.

(43) Armstrong, W. H.; Lippard, S. J. *J. Am. Chem. Soc.* **1985**, *107*, 3730–3731.

(44) (a) Ben-Hussein, A.; Gomez-Romero, P.; Jameson, G. B., structure of compound reported in ref 44b to be submitted for publication. (b) Suzuki, M.; Uehara, A. *Inorg. Chim. Acta* **1986**, *123*, L9–L10.